The hepatitis E virus capsid protein ORF2 counteracts cell-intrinsic antiviral responses to enable persistence in hepatocytes

Ann-Kathrin Mehnert[1,2], Sebastian Stegmaier[2,3#], Carlos Ramirez[4#], Vladimir Gonçalves Magalhães[3], Carla Siebenkotten[1], Jungen Hu[1,2], Ana Luisa Costa[4], Daniel Kirrmaier[5,6], Michael Knop[5,6], Xianfang Wu[7], Thibault Tubiana[8], Carl Herrmann[4], Marco Binder[3], and Viet Loan Dao Thi[1,9*]

[1]Schaller Research Group, Department of Infectious Diseases, Virology, Heidelberg University, Medical Faculty Heidelberg, Heidelberg, Germany; [2]Faculty of Biosciences, Heidelberg University, Heidelberg, Germany; [3]Research Group "Dynamics of Early Viral Infection and the Innate Antiviral Response", Division Virus-Associated Carcinogenesis (D430), German Cancer Research Center (DKFZ), Heidelberg, Germany; [4]Institute for Pharmacy and Molecular Biotechnology, Heidelberg University & BioQuant, Heidelberg, Germany; [5]Center for Molecular Biology of Heidelberg University (ZMBH), Heidelberg, Germany; [6]Division Cell Morphogenesis and Signal Transduction (A260), German Cancer Research Center (DKFZ), Heidelberg, Germany; [7]Infection Biology Program and Department of Cancer Biology, Lerner Research Institute, Cleveland Clinic Foundation, Cleveland, OH, USA; [8]Institute for Integrative Biology of the Cell (I2BC), Université Paris-Saclay, CEA, CNRS, Gif-sur-Yvette, France; [9]German Center for Infection Research (DZIF), Partner Site Heidelberg, Heidelberg, Germany

[#]Authors contributed equally
*Corresponding author: VietLoan.DaoThi@med.uni-heidelberg.de

Classification: Biological Sciences, Microbiology

Keywords: Hepatitis E virus, cell-intrinsic antiviral response, interferon response, viral antagonism, single-cell RNA-sequencing, viral persistence

Electronic word count: 11.441

Number of figures and tables: 4 figures

Abstract

Hepatitis E virus (HEV) is a significant human pathogen causing both acute and chronic infections worldwide. The cell-intrinsic antiviral response serves as the initial defense against viruses and has been shown to be activated upon HEV infection. HEV can replicate in the presence of this response, but the underlying mechanisms remain poorly understood.

Here, we investigated the role of HEV structural proteins ORF2 and ORF3 in immunocompetent cells. Mechanistically, we found that ectopic ORF2, but not ORF3, interfered with inflammatory signaling pathways as well as with antiviral signaling downstream of pattern recognition receptors. The latter was at least in part mediated through direct interaction with the central adaptor protein TANK binding kinase 1. In addition, we discovered a protective mechanism mediated by ORF2 that shielded viral replication from antiviral effectors. Using single-cell RNA-sequencing, we confirmed that the ORF2-mediated antagonism in infected cells resulted in dampened antiviral responses in both HEV-infected and bystander cells. As a consequence, we found that early in the infection process, the progression of authentic HEV infection relied on the presence of ORF2, facilitating a balance between viral replication and the antiviral response within immunocompetent cells. Altogether, our findings shed new light on the multifaceted role of ORF2 in the HEV life cycle and improve our understanding of the determinants that may contribute to HEV persistence.

Significance statement

Hepatitis E virus (HEV) is an important yet often underestimated pathogen. Depending on the genotype, HEV infections can progress to chronicity, but the underlying mechanisms remain poorly understood. To gain insight into potential determinants, we investigated how HEV evades the body's first line of defense, the cell-intrinsic antiviral response. We discovered that the HEV capsid protein ORF2 is crucial in limiting this response by interfering with antiviral signaling pathways and shielding viral replication from immune effectors. This balance between viral replication and the antiviral response contributes to persistent HEV infection in immunocompetent cells. Our findings reveal a new role for the HEV capsid protein in the viral life cycle and highlight it as an important target for novel therapeutic approaches.

Introduction

Hepatitis E virus (HEV) is one of the major causes of acute hepatitis across the globe, affecting an estimated 20 million people every year (reviewed in[1,2]). As part of the *Hepeviridae* family, the *Paslahepevirus balayani* genus comprises eight genotypes of which HEV-1 to HEV-4, and more recently HEV-7, have been associated with human infections. HEV-1 and HEV-2 are transmitted fecal-orally and are restricted to humans. In contrast, HEV-3 and HEV-4 spread to humans zoonotically through consumption of meat products from domestic pigs or wild boar. Although HEV-1/-2 infections are usually self-limiting, they are associated with high mortality in pregnant women. Further, HEV-3 and -4 infection of immunocompromised individuals can result in chronicity and development of liver fibrosis and cirrhosis.

HEV is ingested and excreted as a naked virus but circulates in the bloodstream wrapped in a host membrane-derived quasi-envelope, which is acquired during budding from cells (reviewed in[3]). It has a positive-sense, single-stranded RNA genome of approximately 7.2 kilobases, encompassing three open reading frames (ORFs) that give rise to three viral proteins (reviewed in[2]). ORF1 contains the domains involved in viral replication, such as the RNA-dependent RNA polymerase (RdRp). ORF3 is a small phosphoprotein that mediates secretion of viral progeny.

Three distinct isoforms of ORF2 have been described in HEV-infected cells[4-7]. Owing to its N-terminal signal peptide, ORF2 can be secreted along the secretory pathway where it gives rise to the glycosylated (ORF2g) and cleaved (ORF2c) isoforms. ORF2g is secreted as a dimer[5,6] and serves as an immunological decoy *in vivo*[5]. It has been postulated that positively charged residues within an arginine-rich motif (ARM; five arginine residues: RRRGRR) downstream of the signal peptide assist ORF2 in retaining a cytosolic orientation at the endoplasmic reticulum membrane[4]. This intracellular ORF2 isoform (ORF2i) assembles into infectious progenies. ORF2i is mainly located in the cytosol but can translocate to the nucleus, and is likely involved in many virus-host interactions[4,7]. Another study highlighted the importance of two ORF2 start codons. The first start codon can give rise to the secreted ORF2g, while the second gives rise to ORF2i with intracellular localization[5]. Although it remains unclear whether differential usage of these start codons is relevant in HEV infection, they can be used to abrogate expression of individual or all ORF2 isoforms.

Cell-intrinsic defense strategies are initiated by recognition of pathogen-associated molecular patterns (PAMPs) through pattern recognition receptors (PRRs) (reviewed in[8]). In epithelial cells, double-stranded (ds)RNA, the replication intermediate of RNA viruses, is detected by the family of retinoic acid-inducible gene I (RIG-I)-like receptors (RLRs) in the cytosol, including RIG-I and melanoma differentiation-associated protein 5 (MDA5), which are additionally regulated by laboratory of genetics and physiology 2 (LGP2). In the endosome, Toll-like receptor 3 (TLR3) recognizes dsRNA. Different adaptor proteins mediate downstream signaling: Toll/interleukin-1 receptor (TIR) domain-containing adaptor-inducing interferon-β (TRIF) is recruited by TLR3, while RIG-I and MDA5 induce polymerization of mitochondrial antiviral signaling protein (MAVS). Both result in activation of TANK binding kinase 1 (TBK1) and the inhibitor of nuclear factor-κB (IκB) kinase (IKK) complex. TBK1 phosphorylates interferon regulatory factor 3 (IRF3), which translocates into the nucleus and induces expression of type I and type III interferons (IFNs) and IFN-stimulated genes (ISGs). Autocrine and paracrine IFN signaling through Janus kinase/signal transducers and activators of transcription (JAK/STAT) results in expression of hundreds of ISGs

with antiviral functions (reviewed in[9]). Activation of the IKK complex leads to nuclear translocation of nuclear factor-κB (NF-κB) and expression of inflammatory cytokines.

Despite growing interest and advances in recent years, the cell-intrinsic antiviral response to HEV infection remains poorly described. HEV-infected chimpanzees had a similar but weaker ISG response compared to hepatitis C virus (HCV) infection, likely owing to the lower HEV viremia[10]. *In vitro*, the HEV RNA has been identified as a potent agonist for PRR-mediated IFN induction[11]. As a result, infection of innate immunocompetent hepatocyte models with HEV induced robust type III IFN responses[12,13]. The induced IFN response appeared to be persistent but was unable to eliminate viral replication within the observed time frames[12,13]. Blunting of IFN induction did not result in enhanced viral replication, suggesting that HEV has developed mechanisms to persistently replicate in the presence of a sustained antiviral response[13]. Corroborating this, several studies have shown that HEV replication is relatively resistant to exogenous IFN treatment, as compared to, for example, HCV[12,14-16]. Yin and colleagues proposed that this is the result of an internal IFN refractoriness due to persistent activation of JAK/STAT1 signaling and retention of phosphorylated STAT1 in the cytosol rather than a direct viral antagonism[12].

However, all HEV proteins have previously been suggested to antagonize the cell-intrinsic antiviral response (reviewed in[17]). Within ORF1, the X domain, the putative papain-like cysteine protease (PCP) domain, and the methyltransferase (MeT) domain were shown to interfere with type I IFN induction and NF-κB-mediated signaling[18-21]. A combined MeT-Y-PCP polyprotein was further found to interfere with the JAK/STAT pathway[22]. The ORF2 protein has been reported to interact with TBK1[23,24] and hinder activation of NF-κB[4,25]. Studies of potential ORF3-mediated antagonisms have been controversial: while some studies suggested that ORF3 interferes with type I IFN production, NF-κB-, and IFN-mediated signaling[26-28], one study showed that ORF3 could enhance IFN induction[29]. However, most investigations have relied on overexpression of individual HEV proteins or subdomains of ORF1 and the physiological relevance of each antagonism for HEV replication remains elusive.

In the present study, we sought to clarify the role of HEV ORF2 and ORF3 proteins in antagonizing antiviral responses and their impact on HEV infection. To address this, we made use of viral mutants and assessed differences in IFN and ISG responses upon authentic infection of different immunocompetent hepatocellular systems in bulk and at single-cell resolution. We identified a replication-limiting bottleneck mediated by the antiviral response early in infection that is overcome by the capsid protein ORF2, but not ORF3, allowing for the establishment of persistent viral replication.

Results

The HEV ORF2 protein antagonizes both antiviral and inflammatory signaling pathways and interacts with TBK1

Several studies have suggested that HEV ORF2 and ORF3 antagonize different steps of the cell-intrinsic antiviral response[23-28]. We aimed to validate these findings and first analyzed their interference with the sensing pathway. For this mechanistic investigation, we made use of readily available A549-derived cell lines, which harbor a double knockout of RIG-I and MDA5 and show negligible TLR3 expression[30]. In addition to reconstitution with weak transgene overexpression of either RIG-I[31], MDA5[31], or TLR3, we ectopically expressed HEV ORF2, ORF3, or GFP in these

144 cells. In GFP-expressing cells, stimulation of the respective PRR with Sendai virus (SeV), Mengo-
145 Zn virus, and poly(I:C) supernatant feeding resulted in the induction of *IFNB1* expression (Fig.
146 1A-C). Ectopic expression of HEV ORF3 did not significantly alter *IFNB1* expression downstream
147 of RIG-I and MDA5 (Fig. 1A-B) but resulted in a minor enhancement downstream of TLR3
148 compared to the GFP control (Fig. 1C). In cells expressing ectopic ORF2, *IFNB1* induction was
149 significantly lower downstream of all PRRs compared to GFP-expressing cells (Fig. 1A-C). Not
150 only ORF2 from a chronic HEV genotype (HEV-3) but also from an acute genotype (HEV-1)
151 dampened this response (Fig. 1A-C). By ELISA, we confirmed that ectopic ORF2 expression also
152 decreased IFNβ protein secretion (Suppl. fig. 1A-C). While the presence of ectopic ORF2
153 dampened the strength of *IFNB1* induction, it did not alter the dynamics of RLR signaling, which
154 we tested by time-resolved RT-qPCR analysis of MDA5-expressing cells electroporated with
155 poly(I:C) (Suppl. fig. 1D-E).
156 We further investigated the impact of ORF2 expression on cytokine-dependent antiviral
157 and inflammatory signaling. Upon TNF stimulation, the presence of ectopic ORF2, but not ORF3,
158 reduced the induction of the inflammatory cytokine *TNFAIP3* significantly (Fig. 1D), thus
159 interfering with NF-κB-dependent signaling. On the other hand, we did not observe significant
160 differences in expression of the ISG *IFIT1* upon stimulation with IFNβ in the presence of either
161 ectopic ORF2 or ORF3, suggesting that neither interfered with JAK/STAT signaling (Fig. 1E).
162 In agreement with previous studies, these results confirmed that ORF2 interferes with the
163 sensing pathway upstream of IFN induction[23,24] as well as with NF-κB-dependent inflammatory
164 cytokine induction downstream of the TNF receptor. In contrast, ORF3 did not affect antiviral and
165 inflammatory responses as strongly as proposed previously[26-29]. As NF-κB-dependent cytokine
166 induction is particularly important for the crosstalk with immune cells *in vivo*, we continued
167 focusing on the effects of ORF2 on the antiviral IFN/ISG response.
168 It was previously suggested that ORF2 interacts with the critical adaptor molecule TBK1,
169 likely through the ARM[24], but a direct interaction through this motif was not analyzed. Here, we
170 confirmed the interaction of HEV-3 ORF2 and TBK1 by co-immunoprecipitation (co-IP) (Fig. 1F).
171 We further found that mutation of the last two arginine residues of the ARM to alanine (2R/2A)
172 decreased the interaction of TBK1 with ORF2 (Fig. 1F). However, this particular mutation
173 abrogates nuclear translocation of ORF2i and increases ORF2 secretion and glycosylation along
174 the secretory pathway[4]. Hence, the pool of cytosolic ORF2i is reduced[4] and thus, also the
175 likelihood of interaction with TBK1. In agreement with this, the ORF2-2R/2A protein appeared with
176 a light smear in our Western blot (WB) analysis as compared to WT ORF2, suggesting the
177 presence of post-translational modifications such as glycosylation (Fig. 1F).
178 In an effort to determine other potential interaction motifs between ORF2 and TBK1, we
179 made use of AlphaFold. Repeated modeling identified the last three residues of the LGSA<u>WRD</u>
180 motif (spanning amino acids 83 to 89) at the N-terminus of ORF2 as the only promising, putative
181 interaction motif (Suppl. fig. 2A, 2C-E). However, mutation of these residues to triple alanine did
182 not result in impaired interaction between ORF2 and TBK1, suggesting that this predicted motif
183 is not essential (Suppl. fig. 2B).
184 Altogether, we have shown that ORF2 counteracts IFN induction downstream of all
185 relevant PRRs and additionally interferes with NF-κB-mediated signaling. The antagonism of the
186 antiviral response by ORF2 is mediated, at least in part, by interaction with TBK1, although the
187 precise interaction motif remains elusive.

188
189 *The capsid protein ORF2, but not the ORF3 protein, is pivotal for efficient HEV replication in*
190 *immunocompetent cells*
191 HEV replication in hepatocytes persists in the presence of a sustained cell-intrinsic
192 antiviral response[12,13]. To study how far HEV replication is dependent on ORF2-mediated escape
193 of the antiviral response, we generated a ΔORF2 and a control ΔORF3 mutant of the HEV-3
194 Kernow-C1/p6 (wild-type, WT) strain (Fig. 2A). For the ΔORF2 mutant, we mutated the two start
195 codons of *ORF2* to abrogate protein expression of all ORF2 isoforms without affecting correct
196 translation of the overlapping *ORF3*, as suggested by Yin *et al.*[5]. Upon electroporation (EPO) into
197 immunocompetent HepG2/C3A cells[12,32], we observed significantly reduced replication of the
198 ΔORF2 mutant compared to both WT and the ΔORF3 mutant at day 5 and day 7 post-EPO (Fig.
199 2B). Of note, at least part of the basal HEV RNA detected up to day 3 post-EPO resulted from
200 high levels of incoming, electroporated RNA, as revealed by comparison with a replication-
201 incompetent GNN mutant of the RdRp. Compared to HEV WT, ΔORF2 replication induced a
202 stronger antiviral response, as evidenced by significantly increased *IFNL1* (Fig. 2C) and *ISG15*
203 (Fig. 2D) expression at day 5 and day 7 post-EPO (corresponding non-normalized data in Suppl.
204 fig. 3A-B). Since the ΔORF3 virus replicated at WT levels and ORF3 is the protein responsible for
205 secretion of progeny, we ruled out effects of ORF2 and ORF3 deletion on secondary virus spread.
206 In addition, newly produced virus particles released into the supernatant are quasi-enveloped and
207 therefore, not highly infectious[33].
208 We hypothesized that the antiviral response induced in the absence of ORF2 was strong
209 enough to cause, at least in part, the observed decline in viral replication. In order to address this,
210 we exogenously inhibited IFN and ISG induction by treating the cells with the TBK1 inhibitor
211 BX795. Prolonged incubation with BX795 can affect cell viability, as TBK1 is involved in many
212 cellular processes. To minimize such effects (Suppl. fig. 3C-E), we incubated the cells with BX795
213 for only 48 h before harvesting. Application of BX795 reduced *IFNL1* and *ISG15* induction in
214 response to viral replication (Suppl. fig. 3F-H). HEV WT replication was not significantly enhanced
215 (Fig. 2E), while ΔORF3 replication showed only a minor increase (Fig. 2G). In contrast, the BX795
216 treatment resulted in a significant and stronger increase in ΔORF2 replication (Fig. 2F). This
217 implied that the antiviral response, which peaked at day 5 post-EPO (Fig. 2C), had a greater effect
218 on viral replication in the absence of ORF2, in line with the ORF2-mediated antagonism described
219 above.
220 To study this observation at the single-cell level, we detected HEV genomes by RNA-
221 fluorescence *in situ* hybridization (RNA-FISH), allowing us to quantify the percentage of HEV-
222 infected cells over time, independent of viral antigen expression. As early as day 3 post-EPO,
223 ΔORF2 RNA signals were weaker compared to WT and ΔORF3 and continued to decline
224 thereafter (Fig. 2H-I). Analogous to our results in Fig. 2B, the decrease in WT- and ΔORF3-
225 positive cells from day 3 to day 5 post-EPO was likely due to residual incoming RNA introduced
226 by the EPO process (Fig. 2I). Overall, the percentages of WT- and ΔORF3-positive cells remained
227 comparable between day 5 and day 7 post-EPO (Fig. 2I). In contrast, we barely detected ΔORF2
228 RNA at these days as evidenced by a significant decrease compared to day 3. Interestingly,
229 ΔORF2 RNA was still detectable in our bulk RT-qPCR analysis at these time points (Fig. 2B).
230 Since the RNA-FISH assay is based on the hybridization of 20 probe pairs to an *ORF2* target
231 region spanning approximately 1,000 nucleotides[34], whereas RT-qPCR only amplifies a short

232 sequence stretch of 70 nucleotides, it is possible that we majorly detected degraded ΔORF2
233 genomes by RT-qPCR.
234 Next, we aimed to determine whether the absence of ORF2 resulted in increased
235 sensitivity of viral replication to the action of antiviral effectors. To focus solely on the effects of
236 ISGs, we used Huh7.5 cells, which are only weakly responsive to PRR stimulation due to a non-
237 functional RIG-I and negligible basal expression levels of MDA5[35], TLR3[35], and LGP2[36].
238 Therefore, HEV replication should not induce an antiviral response. Indeed, EPO of Huh7.5 cells
239 with WT and ΔORF2 RNA resulted in comparable viral replication (Suppl. fig. 4A), likely due to
240 the lack of an antiviral response in these cells (Suppl. fig. 4B). Next, we treated WT- and ΔORF2-
241 electroporated Huh7.5 cells four days post-EPO with either IFNλ1 or IFNα2A for 72 h to induce
242 ISG expression. Comparable ISG induction between WT and ΔORF2 further confirmed that ORF2
243 did not interfere with JAK/STAT signaling (Suppl. fig. 4C-D). Importantly, we neither detected
244 *IFNB1* nor *IFNL1* expression upon IFN treatment of WT- and ΔORF2-electroporated cells. Thus,
245 we could exclude the possibility that the IFN treatment led to an upregulation of PRR expression
246 and consequently, an enhanced ISG induction in a positive feedback loop due to enhanced
247 sensing of HEV RNA. Nonetheless, we observed that ΔORF2 replication was more strongly
248 inhibited by IFN treatment and the ensuing ISG response than WT replication (Fig. 2J). We
249 therefore concluded that ORF2 replication was more sensitive to the antiviral effects of ISGs
250 induced by exogenous IFN treatment, even in the absence of a directly virus-induced antiviral
251 response. This additionally contributed to the strong decrease in viral replication in the absence
252 of ORF2 (Fig. 2B).
253 Altogether, we found that the antagonism mediated by ORF2 is critical for efficient HEV
254 replication by dampening the induced antiviral response. Further, the absence of ORF2 resulted
255 in increased sensitivity of HEV replication to the action of ISGs, suggesting additional protective
256 functions of the ORF2 protein, independently of its direct interaction with TBK1.
257
258 *A balance between HEV replication and the antiviral response at an early infection bottleneck is*
259 *essential for sustained viral replication*
260 We next sought to identify the time point at which the presence of ORF2 is decisive for
261 the fate of HEV replication in authentic infection. To this end, we established a trans-
262 complementation system in hepatoma S10-3 cells ectopically expressing ORF2 to produce
263 ΔORF2 virus particles (Fig 3A), similar to a previous study[37]. Ectopic ORF2 expression was
264 comparable to the protein level reached by viral replication after EPO of WT HEV RNA into naïve
265 S10-3 cells (Fig. 3B). We further confirmed by WB that ORF3 but not ORF2 was expressed upon
266 EPO of ΔORF2 RNA into naïve cells (Fig. 3B). We then harvested infectious ΔORF2 particles
267 from ORF2-expressing S10-3 cell lysates to perform HEV infections.
268 Next, we aimed to study the replication dynamics after cell entry in HepG2/C3A cells in a
269 time-resolved manner. We synchronized the infection at equal MOI (30 genome equivalents
270 (GE)/cell) of both WT and ORF2-trans-complemented HEV particles by a binding step for 2 hours
271 (h) at 4 °C and internalization for 8 h at 37 °C, after which the inoculum was removed. We
272 analyzed viral replication and the antiviral response every 8 h between day 1 and day 3 post-
273 internalization and every day (i.e., every 24 h) thereafter by RT-qPCR. Replication of WT and the
274 ΔORF2 mutant peaked at 48±8 h post-internalization, followed by a decline (Fig. 3C).
275 Interestingly, while the HEV WT replication leveled off between 56 h and day 7 post-internalization

276 (2.0-fold decrease), ΔORF2 replication continued to decrease significantly by 8.5-fold between
277 those two time points. With the onset of viral replication, we observed an increase in *IFNL1* (Fig.
278 3D) and *ISG15* (Fig. 3E) expression, which was stronger in ΔORF2 infection relative to HEV RNA
279 (Fig. 3D-E; corresponding absolute HEV RNA genome copies and non-normalized *IFNL1* and
280 *ISG15* expression in Suppl. fig. 5A-C). Following the decrease in HEV WT replication after 56 h,
281 *IFNL1* (Fig. 3D) and *ISG15* (Fig. 3E) expression also decreased, relative to HEV RNA. In contrast,
282 the expression of antiviral response genes remained high upon ΔORF2 infection until day 7 post-
283 internalization.
284 Next, we aimed to validate our findings in a more physiologically relevant hepatocellular
285 system. To this end, we used human pluripotent stem cell-derived hepatocyte-like cells (HLCs)
286 which are permissive to HEV infection[13,33] (Fig. 3F). We infected HLCs at equal MOI (= 30 GE/cell)
287 with HEV WT and ΔORF2 virus particles produced by trans-complementation. Similar to our
288 results in infected HepG2/C3A cells, ΔORF2 showed reduced replication (Fig. 3G) while inducing
289 a stronger antiviral response compared to WT HEV RNA, both in absolute numbers as well as
290 normalized to HEV RNA (Fig. 3H and Suppl. fig. 5D).
291 Overall, our observations suggest that the antagonism mediated by ORF2 is critical for
292 establishing an equilibrium between viral replication and the antiviral response early in infection,
293 allowing HEV to replicate in different immunocompetent hepatocellular systems.
294
295 *scRNA-seq analysis reveals ISG responses in HEV-infected cells and bystanders which are*
296 *dampened in the presence of ORF2*
297 Expression of ISGs can be induced immediately downstream of viral recognition by PRRs
298 (reviewed in[9]). In addition, secreted IFN can lead to amplified ISG induction in an auto- and
299 paracrine manner. In HEV infection, it remains unclear whether IFN and ISG responses observed
300 in bulk analyses such as RT-qPCR are derived from infected cells, uninfected bystanders, or
301 possibly both. ISG responses from uninfected bystanders only could be induced by low levels of
302 IFN secretion from infected cells. Alternatively, viral RNA transfer to neighboring cells via
303 extracellular vesicles could lead to IFN and ISG induction in bystanders, similar to what has been
304 described for HCV and other viruses (reviewed in[38]).
305 To identify the cellular origin of the antiviral response in HEV infection and assess potential
306 differences in the response in the absence of the ORF2-mediated antagonism, we performed
307 single-cell RNA-sequencing (scRNA-seq) using microfluidics-based 3'-targeted 10x Genomics.
308 To this end, we infected HepG2/C3A cells with HEV WT and trans-complemented ΔORF2 virus
309 particles in a synchronized manner as described above and analyzed the cells at 56 h post-
310 internalization. This time point represents the antiviral response-mediated bottleneck we identified
311 to be essential for persistent replication in the presence of ORF2 (Fig. 3C-E). Since the ΔORF2
312 virus replicates to almost undetectable levels at later time points, we only analyzed HEV WT-
313 infected cells at day 7 post-infection.
314 We first performed a gene set enrichment analysis of the HEV WT- and ΔORF2-infected
315 samples compared to the uninfected sample at 56 h, using the hallmark gene sets of the Human
316 MSigDB Collections[39]. Interferon alpha and gamma responses were among the most significantly
317 upregulated gene sets, in both HEV WT and ΔORF2 infection, highlighting that the global
318 response was dominated by differential expression of ISGs (Suppl. fig. 6A-B). Enrichment of
319 oxidative phosphorylation and glycolysis gene sets indicated increased metabolic activity of the

320 infected samples. Analysis of HEV WT infection at day 7 showed that the enriched gene sets
321 were comparable over time and interferon-related responses were still prominently enriched
322 (Suppl. fig. 6C).
323 Next, we clustered the uninfected, HEV WT-, and ΔORF2-infected samples at 56 h based
324 on a list of approximately 400 ISGs published previously by Schoggins *et al.*[40] (Fig. 4A-D). This
325 revealed two major subpopulations in the infected samples (Fig. 4B-C), also at day 7 (Suppl. fig.
326 6D). We concluded that the cells located in the cluster overlapping with the uninfected sample
327 were non-responding cells, characterized by unchanged ISG expression. The cells located in the
328 second cluster showed differential ISG expression compared to the non-responding cells and
329 were thus classified as responders, from here on called the "active cluster" (Fig. 4E). In agreement
330 with the globally enhanced metabolic activity (Suppl. fig. 6A-B), this cluster appeared to be more
331 transcriptionally active, as indicated by an increased number of expressed genes (Fig. 4F) as well
332 as an overall increased number of transcripts (Suppl. fig. 6F). Within the WT- and ΔORF2-infected
333 samples, 28.1% and 17.2% of cells were identified as HEV RNA-positive, respectively (Suppl. fig.
334 6G). Interestingly, we observed that most infected cells of both WT- (Fig. 4G) and ΔORF2-infected
335 samples (Fig. 4H) were located in the active cluster, together with uninfected bystanders. We
336 therefore concluded that both actively infected cells and uninfected bystanders responded by
337 upregulated ISG expression. Although detectable by qRT-PCR (Fig. 3D), we could not detect type
338 III IFN gene expression in the infected samples via scRNA-seq, likely due to low respective
339 numbers of transcripts per cell. Therefore, we could not identify whether only infected cells or also
340 uninfected bystanders were the source of IFN. Nonetheless, we could demonstrate that the ISG
341 response was not fully suppressed in actively infected cells by the ORF2 antagonism.
342 Compared with the infected cells in the active cluster, the few infected cells located within
343 the inactive cluster had lower HEV RNA counts (Suppl. fig. 6H). These cells might be at an earlier
344 stage of infection due to a delayed onset of replication or due to secondary infection, which,
345 however, should be limited at this early time point of infection. Finally, not only uninfected
346 bystanders but also HEV-infected cells still showed enhanced ISG expression and localized to
347 the active cluster at day 7 post-HEV WT infection (Suppl. fig. 6E). This provided further evidence
348 that the establishment of an equilibrium between HEV replication and the antiviral response early
349 in infection is essential for persistent viral replication in an antiviral environment.
350 Next, we sought to examine the specific ISG signatures (i.e., the set of ISGs) induced in
351 actively infected cells and uninfected bystanders upon WT and ΔORF2 infection. First, we
352 observed a globally stronger ISG response in ΔORF2-infected cells and bystanders compared to
353 WT infection (Fig 4I), indicating overall increased IFN production and secretion, despite remaining
354 undetectable by scRNA-seq. We then compared the respective lists of differentially expressed
355 ISGs in the active clusters of WT and ΔORF2 infection and found that out of 243 differentially
356 expressed ISGs, 79.8% overlapped (Fig. 4J and Suppl. table 2). Based on this overlap and
357 previous literature on the upregulation of ISGs in HEV infection of different hepatocellular systems
358 and in chimpanzees[10,12,13,41], we selected a subset of ISGs for further comparison of infected cells
359 and bystanders. Among these common differentially expressed genes, both infected cells and
360 uninfected bystanders in the active cluster of the ΔORF2-infected sample showed a globally
361 stronger expression compared to the respective cell populations of the WT-infected sample (Fig.
362 4K).

363 As summarized in Fig. 4L, we identified both actively infected cells and uninfected
364 bystanders to be the cellular origins of ISG responses at early and later time points of HEV
365 infection. Early in infection, the ORF2 antagonism likely contributes to dampening the ISG
366 induction upon sensing in infected cells. In addition, our data suggests that the presence of ORF2
367 leads to decreased autocrine and paracrine IFN signaling, resulting in dampened ISG responses
368 in both infected cells and bystanders.
369
370 **Discussion**
371 HEV replication has been shown to persist despite a sustained cell-intrinsic antiviral
372 response. However, an in-depth understanding of the underlying mechanisms and the active
373 contribution of a viral antagonism is missing. In this study, we analyzed authentic HEV infection
374 with mutants lacking expression of individual viral proteins at single-cell resolution. We identified
375 a replication-limiting bottleneck imposed by the antiviral response where the presence of ORF2
376 and at least partially, its interaction with the adaptor molecule TBK1 determines whether viral
377 replication declines or equilibrates with the antiviral response.
378
379 *Single-cell analysis uncovers the role of the multifunctional capsid protein for HEV persistence*
380 *amidst an antiviral environment*
381 In the present study, we have shown that the capsid protein ORF2 is a critical viral
382 determinant of HEV replication efficiency. Investigation of the cell-intrinsic antiviral response at
383 the single-cell level revealed that both infected cells and uninfected bystanders are the source of
384 the ISG response in HEV infection. The ISG signatures in both cell types were globally stronger
385 in the absence of ORF2, but not strikingly different from WT infection (Fig. 4J-K). Thus, the ORF2-
386 mediated viral antagonism does not completely suppress antiviral responses within infected cells.
387 Instead, it reduces ISG and presumably IFN induction within infected cells and consequently
388 further ISG induction via autocrine and paracrine IFN signaling. Overall, antiviral responses are
389 dampened below a critical threshold, allowing viral replication and the antiviral response to reach
390 an equilibrium where they can coexist. We propose that this equilibrium is a prerequisite for
391 persistent HEV infection. Future studies are needed to determine whether IFN is produced only
392 by infected cells or also by uninfected bystanders, and to characterize the role of secreted ORF2
393 isoforms in influencing paracrine immune signaling.
394 HEV ORF2 appears to be a multifaceted protein with a wide range of functions affecting
395 different host pathways. In addition to its direct involvement in immune evasion downstream of
396 PRR recognition, we speculate that the capsid protein ORF2 may also exert additional, protective
397 functions. Here, we demonstrate that ORF2 is essential for maintaining the relative resistance of
398 HEV to type I and type III IFN treatment, even in the absence of a virus-induced antiviral response
399 (Fig. 2J). Importantly, we were able to exclude a direct inhibition of IFN signaling by ORF2 (Fig.
400 1E). Therefore, we concluded that the capsid protein additionally contributes to the shielding of
401 replicating RNA from the action of ISGs and potentially also from recognition by PRRs.
402 Most positive-sense RNA viruses replicate in the cytosol and restructure their host cell by
403 inducing host membrane-derived replication compartments (reviewed in[42]). While such replication
404 organelles have not yet been reported for HEV, several studies have suggested that different
405 compartments of the endolysosomal system or the ER-Golgi intermediate compartment (ERGIC)
406 could be involved[43-46]. ORF2 was frequently detected at these proposed replication sites.

407 Therefore, it may be involved in either remodeling or redirecting cellular structures to help create
408 the replication site, thereby potentially contributing to protection of viral RNA from the antiviral
409 effects of induced ISGs.
410 Despite the relatively low abundance of ORF1 and ORF3 proteins compared to ORF2
411 protein in authentic infection[47], we cannot exclude the possibility that these proteins have
412 additional potential to interfere with antiviral signaling and contribute to viral persistence. In this
413 study, we did not observe any striking effects of ORF3 on viral replication and antiviral responses.
414 Ectopically expressed ORF3 may interact with components of the antiviral response as reported
415 by others[26-28]. Furthermore, the processing of the ORF1 polyprotein in authentic infection remains
416 controversial (reviewed in[48]). Therefore, physiologically relevant contributions of the previously
417 reported antagonisms by ORF1 to the overall persistence phenotype remain to be confirmed.
418
419 *The direct interaction of HEV ORF2 with TBK1 is critical for antagonizing replication-limiting*
420 *responses*
421 There is no convincing evidence for a viral protease encoded by the HEV genome. Indeed,
422 unlike HCV[49] or HAV[50], HEV does not cleave MAVS[12], a key adaptor molecule in the induction of
423 cell-intrinsic antiviral responses. Instead, HEV appears to have developed other counteraction
424 strategies. In agreement with previous literature[23,24], we found that the HEV ORF2 protein
425 interacts directly with TBK1 to dampen IFN induction and the establishment of an infection-limiting
426 antiviral state. Here, we identified an early time point at which the ORF2-mediated antagonism is
427 critical for the progression of authentic HEV infection, facilitating a balance between viral
428 replication and the antiviral response within immunocompetent cells.
429 Lin and colleagues[24] previously suggested that the ARM of ORF2 is responsible for the
430 inhibition of TBK1-induced phosphorylation of IRF3. Indeed, we could show a reduced interaction
431 between ORF2 and TBK1 upon mutation of the ARM. However, this motif has also been identified
432 as the master regulator of the ORF2 isoforms[4]. Therefore, mutating the ARM could also indirectly
433 affect interference with the antiviral response, as enhanced secretion of glycosylated ORF2 along
434 the secretory pathway results in decreased cytosolic and nuclear availability of ORF2 to interact
435 with TBK1 and other unidentified factors. Furthermore, we found that ORF2 also antagonizes NF-
436 κB-dependent cytokine induction (Fig. 1D) and is hence likely to interfere with additional
437 components other than TBK1. This observation is in agreement with the previously published
438 interaction of ORF2 with beta-transducin repeat containing protein (βTRCP)[25], which resulted in
439 reduced proteasomal degradation of the inhibitory complex of NF-κB. Additionally, nuclear
440 translocation of ORF2 has been proposed to affect inflammatory cytokine induction[4]. Considering
441 the numerous suggested ORF2 antagonisms by us and others, we believe that viral persistence
442 is likely based on combinatorial interference of ORF2 with different pathways.
443 Due to the apparent multifunctionality of the ORF2 protein, individual functions are difficult
444 to untangle if specialized domains remain unknown. Indeed, our attempts to predict any putative
445 interaction sites between ORF2 and TBK1 with AlphaFold remained unsuccessful. The only
446 promising prediction was localized to the N-terminus of ORF2, however, this portion of the ORF2
447 protein appears to be intrinsically disordered[51]. While AlphaFold has demonstrated success in
448 identifying binding regions between other viral proteins and host factors[52], this particular
449 interaction highlights the challenges of accurately predicting interactions involving disordered
450 protein regions[53,54]. This complexity could stem from several factors: AlphaFold heavily relies on

451 co-evolutionary signals, which might be less pronounced in this virus-host interaction.
452 Furthermore, the ORF2-TBK1 interaction may rather be driven by physico-chemical properties
453 that are not explicitly considered in AlphaFold's predictions. Finally, the N-terminus of ORF2 may
454 adopt a specific structure upon interaction with TBK1, as is the case for many intrinsically
455 disordered proteins (reviewed in[55]). High-resolution structural studies of TBK1-ORF2 complexes
456 may therefore be required to further identify the interacting regions.
457
458 *Innate immunity as a potential determinant of HEV chronicity and species tropism*
459 Infections with different HEV genotypes result in distinct clinical outcomes. While HEV-1
460 infections are acute and self-limiting, HEV-3 infections can become chronic in
461 immunocompromised individuals. The determinants of these intergenotypic differences remain to
462 be elucidated, but innate and adaptive immune responses are likely critical parameters (reviewed
463 in[17]).
464 We have previously shown that infection with an HEV-1 isolate resulted in a stronger IFN
465 and ISG response than infection with an HEV-3 isolate. Interestingly, HEV-1 but not HEV-3
466 replication appeared to decrease thereafter[13]. Why HEV-1 induces a stronger response and
467 whether this contributes to the self-limiting course of infection observed in humans and in HEV-
468 1-infected chimpanzees[10] should be investigated in the future.
469 On the other hand, a moderate but prolonged cell-intrinsic IFN response induced by HEV-
470 3 could help to induce tolerance and dampen the effect of the stronger type I IFN response elicited
471 by professional immune cells such as plasmacytoid dendritic cells (pDCs). In agreement, we and
472 others have demonstrated a remarkable resistance of HEV replication to exogenous IFN once
473 replication is fully established[12,14-16]. Continuous activation of JAK/STAT signaling upon HEV
474 replication has been shown to render the cells refractory to exogenous IFN stimulation[12]. A recent
475 publication further suggested that ORF2 isoforms modulate detection of HEV-infected cells by
476 pDCs, indicating that this cell type might be contributing to HEV control *in vivo*[32]. Not only do pDCs
477 produce IFN and other cytokines to activate innate immune cells, but they also capture and
478 process antigens to initiate adaptive T cell responses. Consequently, a reduced T cell activation
479 could be beneficial for establishing HEV persistence *in vivo*.
480 Our results showed no difference in the potential of ORF2 from acute and chronic
481 genotypes to interfere with IRF3- and NF-κB-mediated signaling (Figure 1), which is consistent
482 with previous studies[23,24]. Therefore, the potency of ORF2 to antagonize these signaling pathways
483 does not appear to be a critical factor for the potential of HEV-3 to progress to chronic infection.
484 However, it could play a role in the genotype-dependent species tropism of HEV. While HEV-1 is
485 limited to primates and human infection, HEV-3 can infect a wide range of animals and is mainly
486 transmitted zoonotically to humans. Interaction of ORF2 with TBK1 could potentially represent a
487 prime example of the ongoing arms race between virus and host, driving the co-evolution of viral
488 evasion strategies and host defenses. Therefore, future research should investigate the
489 differences in the ability of HEV-1 and HEV-3 ORF2 to counteract TBK1 from different HEV-3 host
490 species, including pig or rabbit. Such studies will be crucial in identifying the determinants of HEV
491 species tropism.
492 Many open questions remain about the mechanisms of HEV persistence. In this study, we
493 have shown that the HEV capsid protein ORF2 mediates a viral antagonism affecting both antiviral
494 and inflammatory signaling. ORF2 is essential at a replication-limiting bottleneck early in infection

495 mediated by the antiviral response, which is decisive for establishment of persistent viral
496 replication. We have also laid the groundwork for future studies to focus on the role of
497 intergenotypic differences in the antiviral response and crosstalk with immune cells. This could
498 lead to a better understanding of the determinants of acute and chronic manifestations of HEV
499 infection, which will be valuable in identifying novel therapeutic regimens.
500
501 **Materials and Methods**
502 *Standard cell culture*
503 The human hepatoma cell lines HepG2/C3A (ATCC HB-8065), Huh7.5 (a kind gift from
504 Charles Rice, The Rockefeller University), S10-3 (a kind gift from Suzanne Emerson, NIH), and
505 derived S10-3/ORF2 as well as the human embryonic kidney cell line HEK293T (ATCC CRL-
506 3216) were cultured in Dulbecco's Modified Eagle Medium (DMEM, Gibco, high glucose,
507 GlutaMAX supplement) with 10% fetal bovine serum (FBS, Capricorn) and 1%
508 penicillin/streptomycin (pen/strep), referred to as complete DMEM (cDMEM). HepG2/C3A cells
509 were grown on collagen-coated cell culture plasticware. A549-derived cell lines were cultured in
510 DMEM (Gibco, high glucose) with 10% FBS (Pan Biotech), 1% pen/strep, and 1% non-essential
511 amino acids (NEAA). Cell lines with ectopic protein expression were produced by standard
512 lentiviral transduction, selected, and continuously cultured under respective antibiotic selection
513 pressure. Cells were maintained at 37 °C in 95% humidity and 5% CO_2 atmosphere. All cell lines
514 used in this study routinely tested negative for mycoplasma.
515
516 *Stimulation of PRR-overexpressing A549-derived cell lines*
517 $1x10^5$ A549-derived cell lines were seeded in 24-well plates. The next day, cells were
518 infected with Sendai virus (SeV, MOI 0.75; prepared from allantoic fluid of embryonated chicken
519 eggs, a kind gift from Rainer Zawatzky, German Cancer Research Center (DKFZ), Heidelberg,
520 Germany) for 4 h, Mengo-Zn virus[56] (MOI 1) for 24 h, or supernatant-fed with poly(I:C) (InvivoGen)
521 at 50 µg/mL for 24 h in DMEM containing 2% FBS, 1% NEAA, and 1% pen/strep. Stimulation with
522 TNF (Abcam) at 10 ng/mL or IFNβ (R&D Systems) at 200 IU/mL was performed in cDMEM plus
523 1% NEAA for 8 h. At respective time points, cells were lysed for RNA extraction with Monarch
524 Total RNA Miniprep Kit (New England Biolabs).
525
526 *Generation of HEV ΔORF2, ΔORF3, and GNN mutants*
527 Mutants were generated in the plasmid pBlueScript SK(+) encoding the HEV-3 Kernow-
528 C1/p6 sequence (pBSK-HEV-p6, GenBank accession number: JQ679013.1) by site-directed
529 mutagenesis. Mutations were introduced by overlap extension PCR with Phusion or Q5
530 polymerase (New England Biolabs) using the primers listed in Table 1, followed by restriction
531 enzyme digestion (New England Biolabs), ligation with T4 DNA Ligase (New England Biolabs),
532 transformation of JM109 competent cells (Promega), and validation by Sanger DNA sequencing.
533
534 In vitro *transcription and EPO of HEV WT, ΔORF2, ΔORF3, and GNN mutants*
535 Plasmids were linearized with MluI and RNA was *in vitro* transcribed using the
536 mMESSAGE mMACHINE T7 kit (Invitrogen). $4x10^6$ HepG2/C3A cells were electroporated with
537 10 µg of IVT HEV RNA in cytomix (120 mM KCl, 0.15 mM $CaCl_2$, 10 mM KPO_4, 25 mM HEPES,
538 2 mM EGTA, and 5 mM $MgCl_2$), supplemented with adenosine triphosphate (ATP) and glutathione

539 (GT). After resuspension in cDMEM, HepG2/C3A cells electroporated with HEV WT or mutants
540 were mixed 1:1 with mock-electroporated cells. $2x10^5$ cells/well were seeded on 24-well plates
541 for analysis by RT-qPCR and $1x10^5$ cells/well were seeded on 48-well plates for analysis by RNA-
542 FISH. One day post-EPO, all wells were washed twice with PBS to remove inoculum and cDMEM
543 was replaced. Cell lysates were harvested for RNA extraction using the Universal RNA kit
544 (Roboklon) according to manufacturer's instructions. On day 1, day 3, and day 5 post-EPO,
545 cDMEM was replaced and 6 µM TBK1 inhibitor BX795 (InvivoGen) or corresponding DMSO
546 vehicle control was added to the wells dedicated to cell lysis 48 h later. Samples for RNA-FISH
547 were fixed at respective time points with 4% paraformaldehyde (PFA).
548
549 *EPO of Huh7.5 cells and IFN treatment*
550 Huh7.5 cells were electroporated with HEV WT or ΔORF2 IVT RNA as described above.
551 For time-course analysis, electroporated Huh7.5 cells were resuspended in cDMEM, seeded in
552 24-well plates, and harvested for RT-qPCR analysis at respective time points. For IFN treatment,
553 cells were plated in a T75 cell culture flask. On day 3 post-EPO, cells were reseeded to 24-well
554 plates at approximately 80% confluency. One day later, cells were treated with 10,000 IU/mL
555 IFNα2A or 10 ng/mL IFNλ1. IFNs were replenished daily until cells were lysed for RNA extraction
556 with the Universal RNA kit (Roboklon) and RT-qPCR on day 7 post-EPO.
557
558 *ΔORF2 virus production by trans-complementation*
559 S10-3/ORF2 cells were electroporated with IVT ΔORF2 RNA and expanded on day 3 post-
560 EPO. Intracellular nHEV particles were harvested 7 days post-EPO from cell lysates by four
561 repeated freeze-thaw cycles and pelleted by ultracentrifugation at 28,000 rpm for 3 h through a
562 20% sucrose cushion. HEV ΔORF2 genome copies were determined by RT-qPCR following
563 TRIzol extraction from the resuspended virus prep.
564
565 *Synchronized, time-resolved HEV infection*
566 $6x10^4$ HepG2/C3A cells were seeded on collagen-coated 24-well plates. The next day,
567 cells were infected with equal genome copies of HEV WT or ΔORF2 virus (30 GE/cell). Virus was
568 bound at 4 °C for 2 h in Minimum Essential Medium (MEM, Gibco), supplemented with 10% FBS
569 and 1% pen/strep, followed by internalization at 37 °C for 8 h. After internalization, inoculum was
570 removed, cells were washed twice with PBS, and cDMEM was added. Samples for RT-qPCR
571 were lysed at respective time points with TRIzol for RNA extraction.
572
573 *3'-targeted 10x Genomics and Illumina sequencing*
574 $8x10^4$ HepG2/C3A cells were seeded on collagen-coated 24-well plates, and synchronized
575 HEV infection was performed as described above. At 56 h and day 7 post-internalization, cells
576 were trypsinized for 10 min, gently resuspended, and singularized by pipetting thrice through a
577 70 µm cell strainer. Two wells of each sample were combined. Single-cell suspensions were
578 washed once with 0.04% BSA in PBS and finally resuspended in 0.04% BSA/PBS. Cell
579 suspension was counted and inspected for cell death using trypan blue. Single-cell suspensions
580 were loaded onto the 10x Chromium controller according to manufacturer's instructions of the
581 Chromium Next GEM Single Cell 3' Kit v3.1 (10x Genomics) with a targeted cell recovery of 5,000.
582 Sequencing libraries were prepared according to the manufacturer's instructions. Briefly, GEMs

were generated, reverse transcription was performed, GEMs were cleaned up, and cDNA was amplified and cleaned up with SPRIselect beads (Beckman Coulter). Quantification and quality control were performed with Qubit (Thermo Fisher Scientific) and the 5200 Fragment Analyzer System (Agilent Technologies). Fragmentation, end repair, and A-tailing were followed by SPRIselect-based cleanup, adaptor ligation, sample indexing, and again, SPRIselect cleanup. Quantification and quality control were performed with 5200 Fragment Analyzer System (Agilent Technologies) and NEBNext Library Quant Kit for Illumina (New England Biolabs). Resulting libraries were pooled and sequenced on Illumina NextSeq550 (high-output mode, paired-end, 150 cycles).

scRNA-seq data analysis

Fastq files were aligned and counted using the Cell Ranger 7.1.0 pipeline. As a human genome reference we used GRCh38-3.0.0. For clustering and UMAP projections, we used only a subset of genes based on a list of ISGs reported by Schoggins *et al.*[40]. Counts were scaled and log1-normalized. The UMAP projections were calculated over the first 20 dimensions of the PCA, setting the following parameters: min.dist=0.5 and n.neighbors=200. In order to identify clusters associated with transcriptionally active/inactive states, we set a resolution of 0.1 in the FindClusters function and then we inspected the expression of ISGs in the identified clusters. For the DEA we used the FindMarkers function and filtered out genes expressed in less than 5% of cells in the compared conditions and with p-adjusted values less than 0.05. For ISG expression we used AUC values to score cells based on the Schoggins signature mentioned above implemented with the AUCell 1.24.0 R package. For the comparison of the gene expression across conditions we used a two-sided Wilcoxon rank sum test. Binarized ORF2 expression was carried out by defining positive cells as those expressing at least one HEV RNA count. We used the Seurat 5.0 R package for the entire analysis. The data is accessible under the GEO accession number GSE288400.

Statistical analysis

Graphs were made and statistical analysis was performed using GraphPad Prism 8 or R 4.3.3 for the scRNA-seq analysis. Statistical tests and p-values are listed in the respective figure legends.

Acknowledgments

The authors gratefully acknowledge Dr. Suzanne Emerson, Dr. Rainer Ulrich, Dr. Frauke Mücksch, and Dr. Henrik Kaessmann for sharing reagents and Andrew Freistaedter and Céline Schneider for excellent technical support. We acknowledge Dr. Vibor Laketa, head of the Infectious Diseases Imaging Platform (IDIP) at the University Hospital Heidelberg for expert support. The authors thank Dr. Marlène Dreux for critical reading of the manuscript. We thank the BIOI2 platform and the I2BC's IT support team for making AlphaFold 2.3 easily accessible at the I2BC.

Funding

A.M., S.S., C.R., C.H., M.B., and V.L.D.T were supported by grants from the Deutsche Forschungsgemeinschaft (DFG, German Research Foundation) – Projektnummer – 272983813 SFB/TRR 179. V.L.D.T. was additionally supported by the Chica and Heinz Schaller Foundation, DFG grant DA1640/3-1, and TTU Hepatitis Project 05.823. J.H. was supported by a fellowship from the China Scholarship Council.

Author contributions

Conceptualization, A.M., and V.L.D.T.; Methodology, A.M., S.S., C.R, V.G.M, C.S., A.L.C., J.H., and T.T.; Investigation, A.M., S.S, C.R., and T.T.; Resources: D.K., M.K., X.W.; Software, A.M., S.S., C.R., A.L.C., T.T.; Data analysis, A.M., S.S., C.R., A.L.C., C.H., J.H.; Writing original draft, A.M., and V.L.D.T.; Final draft, A.M., and V.L.D.T.; Supervision, C.H., B.M., V.L.D.T.; Funding, V.L.D.T.

Declaration of interests

All authors declare no conflict of interest

640 **References**

641 1 Horvatits, T., Schulze Zur Wiesch, J., Lütgehetmann, M., Lohse, A. W. & Pischke, S. The
642 Clinical Perspective on Hepatitis E. *Viruses* **11**, doi:10.3390/v11070617 (2019).
643 2 Nimgaonkar, I., Ding, Q., Schwartz, R. E. & Ploss, A. Hepatitis E virus: advances and
644 challenges. *Nat Rev Gastroenterol Hepatol* **15**, 96-110, doi:10.1038/nrgastro.2017.150
645 (2018).
646 3 Das, A., Rivera-Serrano, E. E., Yin, X., Walker, C. M., Feng, Z. & Lemon, S. M. Cell entry
647 and release of quasi-enveloped human hepatitis viruses. *Nature reviews. Microbiology* **21**,
648 573-589, doi:10.1038/s41579-023-00889-z (2023).
649 4 Hervouet, K., Ferrie, M., Ankavay, M., Montpellier, C., Camuzet, C., Alexandre, V.,
650 Dembele, A., Lecoeur, C., Foe, A. T., Bouquet, P., Hot, D., Vausselin, T., Saliou, J. M.,
651 Salome-Desnoulez, S., Vandeputte, A., Marsollier, L., Brodin, P., Dreux, M., Rouille, Y.,
652 Dubuisson, J., Aliouat-Denis, C. M. & Cocquerel, L. An Arginine-Rich Motif in the ORF2
653 capsid protein regulates the hepatitis E virus lifecycle and interactions with the host cell.
654 *PLoS Pathog* **18**, e1010798, doi:10.1371/journal.ppat.1010798 (2022).
655 5 Yin, X., Ying, D., Lhomme, S., Tang, Z., Walker, C. M., Xia, N., Zheng, Z. & Feng, Z.
656 Origin, antigenicity, and function of a secreted form of ORF2 in hepatitis E virus infection.
657 *Proc Natl Acad Sci U S A* **115**, 4773-4778, doi:10.1073/pnas.1721345115 (2018).
658 6 Montpellier, C., Wychowski, C., Sayed, I. M., Meunier, J. C., Saliou, J. M., Ankavay, M.,
659 Bull, A., Pillez, A., Abravanel, F., Helle, F., Brochot, E., Drobecq, H., Farhat, R., Aliouat-
660 Denis, C. M., Haddad, J. G., Izopet, J., Meuleman, P., Goffard, A., Dubuisson, J. &
661 Cocquerel, L. Hepatitis E Virus Lifecycle and Identification of 3 Forms of the ORF2 Capsid
662 Protein. *Gastroenterology* **154**, 211-223 e218, doi:10.1053/j.gastro.2017.09.020 (2018).
663 7 Ankavay, M., Montpellier, C., Sayed, I. M., Saliou, J. M., Wychowski, C., Saas, L., Duvet,
664 S., Aliouat-Denis, C. M., Farhat, R., de Masson d'Autume, V., Meuleman, P., Dubuisson,
665 J. & Cocquerel, L. New insights into the ORF2 capsid protein, a key player of the hepatitis
666 E virus lifecycle. *Sci Rep* **9**, 6243, doi:10.1038/s41598-019-42737-2 (2019).
667 8 Wu, J. & Chen, Z. J. Innate immune sensing and signaling of cytosolic nucleic acids. *Annu*
668 *Rev Immunol* **32**, 461-488, doi:10.1146/annurev-immunol-032713-120156 (2014).
669 9 Schneider, W. M., Chevillotte, M. D. & Rice, C. M. Interferon-stimulated genes: a complex
670 web of host defenses. *Annu Rev Immunol* **32**, 513-545, doi:10.1146/annurev-immunol-
671 032713-120231 (2014).
672 10 Yu, C., Boon, D., McDonald, S. L., Myers, T. G., Tomioka, K., Nguyen, H., Engle, R. E.,
673 Govindarajan, S., Emerson, S. U. & Purcell, R. H. Pathogenesis of hepatitis E virus and
674 hepatitis C virus in chimpanzees: similarities and differences. *J Virol* **84**, 11264-11278,
675 doi:10.1128/JVI.01205-10 (2010).
676 11 Sooryanarain, H., Heffron, C. L. & Meng, X. J. The U-Rich Untranslated Region of the
677 Hepatitis E Virus Induces Differential Type I and Type III Interferon Responses in a Host
678 Cell-Dependent Manner. *mBio* **11**, doi:10.1128/mBio.03103-19 (2020).
679 12 Yin, X., Li, X., Ambardekar, C., Hu, Z., Lhomme, S. & Feng, Z. Hepatitis E virus persists
680 in the presence of a type III interferon response. *PLoS Pathog* **13**, e1006417,
681 doi:10.1371/journal.ppat.1006417 (2017).
682 13 Wu, X., Dao Thi, V. L., Liu, P., Takacs, C. N., Xiang, K., Andrus, L., Gouttenoire, J.,
683 Moradpour, D. & Rice, C. M. Pan-Genotype Hepatitis E Virus Replication in Stem Cell-
684 Derived Hepatocellular Systems. *Gastroenterology* **154**, 663-674 e667,
685 doi:10.1053/j.gastro.2017.10.041 (2018).
686 14 Dao Thi, V. L., Debing, Y., Wu, X., Rice, C. M., Neyts, J., Moradpour, D. & Gouttenoire, J.
687 Sofosbuvir Inhibits Hepatitis E Virus Replication In Vitro and Results in an Additive Effect
688 When Combined With Ribavirin. *Gastroenterology* **150**, 82-85 e84,
689 doi:10.1053/j.gastro.2015.09.011 (2016).

690 15 Todt, D., Francois, C., Anggakusuma, Behrendt, P., Engelmann, M., Knegendorf, L.,
691 Vieyres, G., Wedemeyer, H., Hartmann, R., Pietschmann, T., Duverlie, G. & Steinmann,
692 E. Antiviral Activities of Different Interferon Types and Subtypes against Hepatitis E Virus
693 Replication. *Antimicrob Agents Chemother* **60**, 2132-2139, doi:10.1128/AAC.02427-15
694 (2016).
695 16 Debing, Y., Emerson, S. U., Wang, Y., Pan, Q., Balzarini, J., Dallmeier, K. & Neyts, J.
696 Ribavirin inhibits in vitro hepatitis E virus replication through depletion of cellular GTP
697 pools and is moderately synergistic with alpha interferon. *Antimicrob Agents Chemother*
698 **58**, 267-273, doi:10.1128/aac.01795-13 (2014).
699 17 Bruggemann, Y., Klohn, M., Wedemeyer, H. & Steinmann, E. Hepatitis E virus: from innate
700 sensing to adaptive immune responses. *Nat Rev Gastroenterol Hepatol*,
701 doi:10.1038/s41575-024-00950-z (2024).
702 18 Nan, Y., Yu, Y., Ma, Z., Khattar, S. K., Fredericksen, B. & Zhang, Y. J. Hepatitis E virus
703 inhibits type I interferon induction by ORF1 products. *J Virol* **88**, 11924-11932,
704 doi:10.1128/jvi.01935-14 (2014).
705 19 Kang, S., Choi, C., Choi, I., Han, K. N., Rho, S. W., Choi, J., Kwon, J., Park, M. K., Kim,
706 S. J. & Myoung, J. Hepatitis E Virus Methyltransferase Inhibits Type I Interferon Induction
707 by Targeting RIG-I. *J Microbiol Biotechnol* **28**, 1554-1562, doi:10.4014/jmb.1808.08058
708 (2018).
709 20 Kim, E. & Myoung, J. Hepatitis E Virus Papain-Like Cysteine Protease Inhibits Type I
710 Interferon Induction by Down-Regulating Melanoma Differentiation-Associated Gene 5. *J*
711 *Microbiol Biotechnol* **28**, 1908-1915, doi:10.4014/jmb.1809.09028 (2018).
712 21 Myoung, J. & Min, K. Dose-Dependent Inhibition of Melanoma Differentiation-Associated
713 Gene 5-Mediated Activation of Type I Interferon Responses by Methyltransferase of
714 Hepatitis E Virus. *J Microbiol Biotechnol* **29**, 1137-1143, doi:10.4014/jmb.1905.05040
715 (2019).
716 22 Bagdassarian, E., Doceul, V., Pellerin, M., Demange, A., Meyer, L., Jouvenet, N. & Pavio,
717 N. The Amino-Terminal Region of Hepatitis E Virus ORF1 Containing a Methyltransferase
718 (Met) and a Papain-Like Cysteine Protease (PCP) Domain Counteracts Type I Interferon
719 Response. *Viruses* **10**, doi:10.3390/v10120726 (2018).
720 23 Hingane, S., Joshi, N., Surjit, M. & Ranjith-Kumar, C. T. Hepatitis E Virus ORF2 Inhibits
721 RIG-I Mediated Interferon Response. *Front Microbiol* **11**, 656,
722 doi:10.3389/fmicb.2020.00656 (2020).
723 24 Lin, S., Yang, Y., Nan, Y., Ma, Z., Yang, L. & Zhang, Y. J. The Capsid Protein of Hepatitis
724 E Virus Inhibits Interferon Induction via Its N-terminal Arginine-Rich Motif. *Viruses* **11**,
725 doi:10.3390/v11111050 (2019).
726 25 Surjit, M., Varshney, B. & Lal, S. K. The ORF2 glycoprotein of hepatitis E virus inhibits
727 cellular NF-κB activity by blocking ubiquitination mediated proteasomal degradation of
728 IκBα in human hepatoma cells. *BMC biochemistry* **13**, 7, doi:10.1186/1471-2091-13-7
729 (2012).
730 26 Dong, C., Zafrullah, M., Mixson-Hayden, T., Dai, X., Liang, J., Meng, J. & Kamili, S.
731 Suppression of interferon-alpha signaling by hepatitis E virus. *Hepatology* **55**, 1324-1332,
732 doi:10.1002/hep.25530 (2012).
733 27 He, M., Wang, M., Huang, Y., Peng, W., Zheng, Z., Xia, N., Xu, J. & Tian, D. The ORF3
734 Protein of Genotype 1 Hepatitis E Virus Suppresses TLR3-induced NF-kappaB Signaling
735 via TRADD and RIP1. *Sci Rep* **6**, 27597, doi:10.1038/srep27597 (2016).
736 28 Lei, Q., Li, L., Zhang, S., Li, T., Zhang, X., Ding, X. & Qin, B. HEV ORF3 downregulates
737 TLR7 to inhibit the generation of type I interferon via impairment of multiple signaling
738 pathways. *Sci Rep* **8**, 8585, doi:10.1038/s41598-018-26975-4 (2018).

739 29 Nan, Y., Ma, Z., Wang, R., Yu, Y., Kannan, H., Fredericksen, B. & Zhang, Y. J.
740 Enhancement of interferon induction by ORF3 product of hepatitis E virus. *J Virol* **88**, 8696-
741 8705, doi:10.1128/jvi.01228-14 (2014).
742 30 Plociennikowska, A., Frankish, J., Moraes, T., Del Prete, D., Kahnt, F., Acuna, C., Slezak,
743 M., Binder, M. & Bartenschlager, R. TLR3 activation by Zika virus stimulates inflammatory
744 cytokine production which dampens the antiviral response induced by RIG-I-like receptors.
745 *J Virol* **95**, doi:10.1128/JVI.01050-20 (2021).
746 31 Magalhães, V. G., Lukassen, S., Drechsler, M., Loske, J., Burkart, S. S., Wüst, S.,
747 Jacobsen, E. M., Röhmel, J., Mall, M. A., Debatin, K. M., Eils, R., Autenrieth, S., Janda,
748 A., Lehmann, I. & Binder, M. Immune-epithelial cell cross-talk enhances antiviral
749 responsiveness to SARS-CoV-2 in children. *EMBO reports* **24**, e57912,
750 doi:10.15252/embr.202357912 (2023).
751 32 Joshi, G., Décembre, E., Brocard, J., Montpellier, C., Ferrié, M., Allatif, O., Mehnert, A.-
752 K., Pons, J., Galiana, D., Dao Thi, V. L., Jouvenet, N., Cocquerel, L. & Dreux, M. Hepatitis
753 E Virus-induced antiviral response by plasmacytoid dendritic cells is modulated by the
754 ORF2 protein. 2024.2004.2012.589258, doi:10.1101/2024.04.12.589258 %J bioRxiv
755 (2024).
756 33 Dao Thi, V. L., Wu, X., Belote, R. L., Andreo, U., Takacs, C. N., Fernandez, J. P., Vale-
757 Silva, L. A., Prallet, S., Decker, C. C., Fu, R. M., Qu, B., Uryu, K., Molina, H., Saeed, M.,
758 Steinmann, E., Urban, S., Singaraja, R. R., Schneider, W. M., Simon, S. M. & Rice, C. M.
759 Stem cell-derived polarized hepatocytes. *Nat Commun* **11**, 1677, doi:10.1038/s41467-
760 020-15337-2 (2020).
761 34 Fu, R., Engels, Z., Weihs, J. A., Mürle, J., Klöhn, M., Todt, D., Hu, J., Steinmann, E.,
762 Böttler, T., Lozach, P.-Y., Lemon, S. M. & Thi, V. L. D. A high-content RNA-based imaging
763 assay reveals integrin beta 1 as a cofactor for cell entry of non-enveloped hepatitis E virus.
764 2023.2010.2027.564362, doi:10.1101/2023.10.27.564362 %J bioRxiv (2023).
765 35 Sumpter, R., Jr., Loo, Y. M., Foy, E., Li, K., Yoneyama, M., Fujita, T., Lemon, S. M. &
766 Gale, M., Jr. Regulating intracellular antiviral defense and permissiveness to hepatitis C
767 virus RNA replication through a cellular RNA helicase, RIG-I. *J Virol* **79**, 2689-2699,
768 doi:10.1128/JVI.79.5.2689-2699.2005 (2005).
769 36 Colasanti, O., Burm, R., Huang, H. E., Riedl, T., Traut, J., Gillich, N., Li, T. F., Corneillie,
770 L., Faure-Dupuy, S., Grünvogel, O., Heide, D., Lee, J. Y., Tran, C. S., Merle, U., Chironna,
771 M., Vondran, F. F. W., Esser-Nobis, K., Binder, M., Bartenschlager, R., Heikenwälder, M.,
772 Meuleman, P. & Lohmann, V. Comparison of HAV and HCV infections in vivo and in vitro
773 reveals distinct patterns of innate immune evasion and activation. *J Hepatol* **79**, 645-656,
774 doi:10.1016/j.jhep.2023.04.023 (2023).
775 37 Ding, Q., Heller, B., Capuccino, J. M., Song, B., Nimgaonkar, I., Hrebikova, G., Contreras,
776 J. E. & Ploss, A. Hepatitis E virus ORF3 is a functional ion channel required for release of
777 infectious particles. *Proc Natl Acad Sci U S A* **114**, 1147-1152,
778 doi:10.1073/pnas.1614955114 (2017).
779 38 Moulin, C., Crupi, M. J. F., Ilkow, C. S., Bell, J. C. & Boulton, S. Extracellular Vesicles and
780 Viruses: Two Intertwined Entities. *Int J Mol Sci* **24**, doi:10.3390/ijms24021036 (2023).
781 39 Liberzon, A., Birger, C., Thorvaldsdottir, H., Ghandi, M., Mesirov, J. P. & Tamayo, P. The
782 Molecular Signatures Database (MSigDB) hallmark gene set collection. *Cell Syst* **1**, 417-
783 425, doi:10.1016/j.cels.2015.12.004 (2015).
784 40 Schoggins, J. W. & Rice, C. M. Interferon-stimulated genes and their antiviral effector
785 functions. *Curr Opin Virol* **1**, 519-525, doi:10.1016/j.coviro.2011.10.008 (2011).
786 41 Todt, D., Friesland, M., Moeller, N., Praditya, D., Kinast, V., Brüggemann, Y., Knegendorf,
787 L., Burkard, T., Steinmann, J., Burm, R., Verhoye, L., Wahid, A., Meister, T. L.,
788 Engelmann, M., Pfankuche, V. M., Puff, C., Vondran, F. W. R., Baumgärtner, W.,
789 Meuleman, P., Behrendt, P. & Steinmann, E. Robust hepatitis E virus infection and

790 transcriptional response in human hepatocytes. *Proc Natl Acad Sci U S A* **117**, 1731-1741,
791 doi:10.1073/pnas.1912307117 (2020).
792 42 de Beijer, N. L., Snijder, E. J. & Bárcena, M. A Cool Look at Positive-Strand RNA Virus
793 Replication Organelles: New Insights from Cryo-Electron Microscopy. *Annual review of*
794 *biochemistry* **93**, 163-187, doi:10.1146/annurev-biochem-052521-115736 (2024).
795 43 Oechslin, N., Da Silva, N., Ankavay, M., Moradpour, D. & Gouttenoire, J. A genome-wide
796 CRISPR/Cas9 screen identifies a role for Rab5A and early endosomes in hepatitis E virus
797 replication. *Proc Natl Acad Sci U S A* **120**, e2307423120, doi:10.1073/pnas.2307423120
798 (2023).
799 44 Bentaleb, C., Hervouet, K., Montpellier, C., Camuzet, C., Ferrie, M., Burlaud-Gaillard, J.,
800 Bressanelli, S., Metzger, K., Werkmeister, E., Ankavay, M., Janampa, N. L., Marlet, J.,
801 Roux, J., Deffaud, C., Goffard, A., Rouille, Y., Dubuisson, J., Roingeard, P., Aliouat-Denis,
802 C. M. & Cocquerel, L. The endocytic recycling compartment serves as a viral factory for
803 hepatitis E virus. *Cell Mol Life Sci* **79**, 615, doi:10.1007/s00018-022-04646-y (2022).
804 45 Metzger, K., Bentaleb, C., Hervouet, K., Alexandre, V., Montpellier, C., Saliou, J. M.,
805 Ferrie, M., Camuzet, C., Rouille, Y., Lecoeur, C., Dubuisson, J., Cocquerel, L. & Aliouat-
806 Denis, C. M. Processing and Subcellular Localization of the Hepatitis E Virus Replicase:
807 Identification of Candidate Viral Factories. *Front Microbiol* **13**, 828636,
808 doi:10.3389/fmicb.2022.828636 (2022).
809 46 Glitscher, M., Spannaus, I. M., Behr, F., Murra, R. O., Woytinek, K., Bender, D. & Hildt, E.
810 The Protease Domain in HEV pORF1 Mediates the Replicase's Localization to
811 Multivesicular Bodies and Its Exosomal Release. *Cell Mol Gastroenterol Hepatol* **17**, 589-
812 605, doi:10.1016/j.jcmgh.2024.01.001 (2024).
813 47 Ankavay, M., Da Silva, N., Pollán, A., Oechslin, N., Dinkelborg, K., Behrendt, P.,
814 Moradpour, D. & Gouttenoire, J. Monitoring of Hepatitis E Virus Infection and Replication
815 by Functional Tagging of the ORF2 Protein. *JHEP Reports*,
816 doi:10.1016/j.jhepr.2024.101293.
817 48 Karpe, Y. A. Processing of the Hepatitis E virus ORF1 nonstructural polyprotein. *Frontiers*
818 *in Virology* **3**, doi:10.3389/fviro.2023.1327745 (2024).
819 49 Meylan, E., Curran, J., Hofmann, K., Moradpour, D., Binder, M., Bartenschlager, R. &
820 Tschopp, J. Cardif is an adaptor protein in the RIG-I antiviral pathway and is targeted by
821 hepatitis C virus. *Nature* **437**, 1167-1172, doi:10.1038/nature04193 (2005).
822 50 Yang, Y., Liang, Y., Qu, L., Chen, Z., Yi, M., Li, K. & Lemon, S. M. Disruption of innate
823 immunity due to mitochondrial targeting of a picornaviral protease precursor. *Proc Natl*
824 *Acad Sci U S A* **104**, 7253-7258, doi:10.1073/pnas.0611506104 (2007).
825 51 Shafat, Z., Ahmed, A., Parvez, M. K. & Parveen, S. Intrinsic disorder in the open reading
826 frame 2 of hepatitis E virus: a protein with multiple functions beyond viral capsid. *Journal,*
827 *genetic engineering & biotechnology* **21**, 33, doi:10.1186/s43141-023-00477-x (2023).
828 52 Ferrie, M., Alexandre, V., Montpellier, C., Bouquet, P., Tubiana, T., Meziere, L., Ankavay,
829 M., Bentaleb, C., Dubuisson, J., Bressanelli, S., Aliouat-Denis, C. M., Rouille, Y. &
830 Cocquerel, L. The AP-1 adaptor complex is essential for intracellular trafficking of the
831 ORF2 capsid protein and assembly of Hepatitis E virus. *Cell Mol Life Sci* **81**, 335,
832 doi:10.1007/s00018-024-05367-0 (2024).
833 53 Bret, H., Gao, J., Zea, D. J., Andreani, J. & Guerois, R. From interaction networks to
834 interfaces, scanning intrinsically disordered regions using AlphaFold2. *Nat Commun* **15**,
835 597, doi:10.1038/s41467-023-44288-7 (2024).
836 54 Versini, R., Sritharan, S., Aykac Fas, B., Tubiana, T., Aimeur, S. Z., Henri, J., Erard, M.,
837 Nüsse, O., Andreani, J., Baaden, M., Fuchs, P., Galochkina, T., Chatzigoulas, A., Cournia,
838 Z., Santuz, H., Sacquin-Mora, S. & Taly, A. A Perspective on the Prospective Use of AI in
839 Protein Structure Prediction. *Journal of chemical information and modeling* **64**, 26-41,
840 doi:10.1021/acs.jcim.3c01361 (2024).

55 Arai, M., Suetaka, S. & Ooka, K. Dynamics and interactions of intrinsically disordered proteins. *Current opinion in structural biology* **84**, 102734, doi:10.1016/j.sbi.2023.102734 (2024).

56 Hato, S. V., Ricour, C., Schulte, B. M., Lanke, K. H., de Bruijni, M., Zoll, J., Melchers, W. J., Michiels, T. & van Kuppeveld, F. J. The mengovirus leader protein blocks interferon-alpha/beta gene transcription and inhibits activation of interferon regulatory factor 3. *Cell Microbiol* **9**, 2921-2930, doi:10.1111/j.1462-5822.2007.01006.x (2007).

Figures

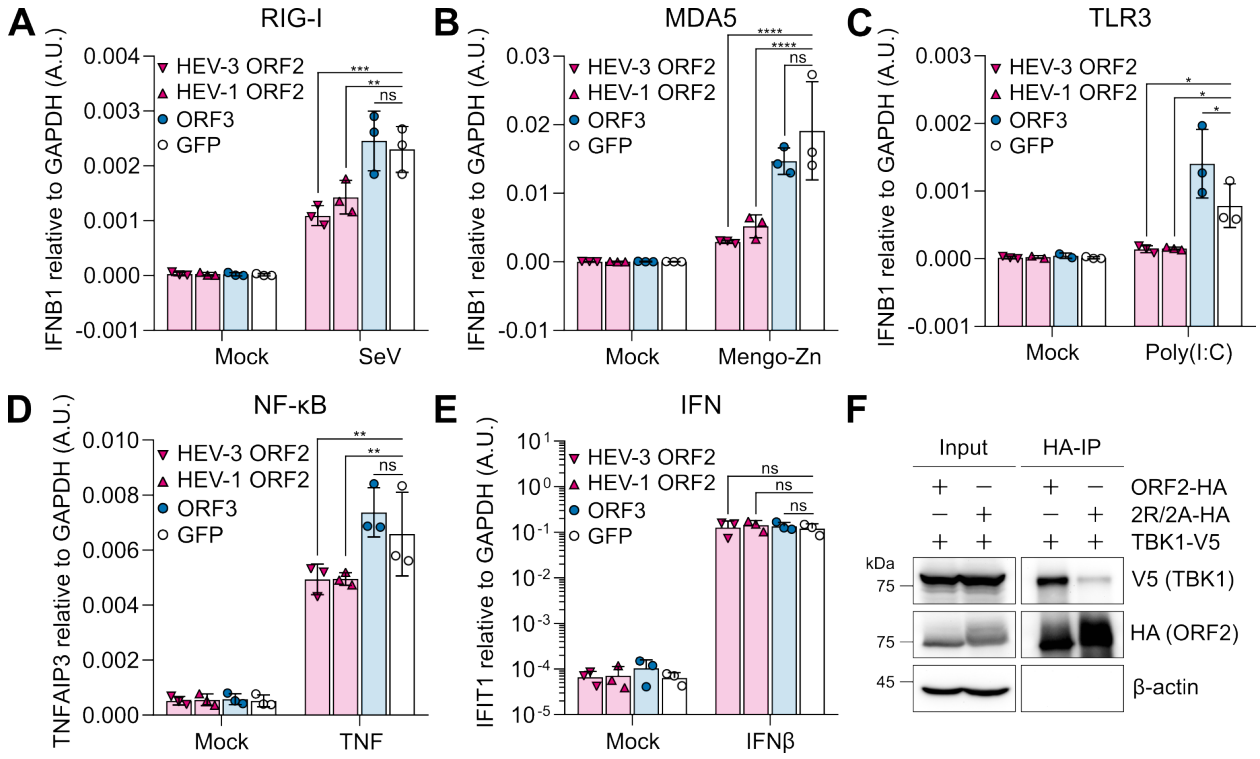

Figure 1: The HEV ORF2 protein antagonizes both antiviral and inflammatory signaling pathways and interacts with TBK1.

(A) A549 cells harboring knockouts of the PRRs RIG-I and MDA5 and ectopically expressing a single PRR (RIG-I, MDA5, or TLR3) together with either HEV-3 ORF2, HEV-1 ORF2, ORF3, or GFP were challenged with either Sendai virus (SeV) for 4 h, (B) Mengo-Zn virus for 24 h, or (C) poly(I:C) supernatant feeding for 24 h, as indicated. (D) A549-derived cells ectopically expressing MDA5 were stimulated with TNF or (E) IFNβ for 8 h. At respective time points, (A-C) *IFNB1*, (D) *TNFAIP3*, and (E) *IFIT1* expression were analyzed by RT-qPCR, each relative to the housekeeping gene *GAPDH*. Data show mean ± SD of n = 3 independent biological experiments. Statistical analysis was performed using two-way ANOVA. *: $p < 0.05$; **: $p < 0.01$; ***: $p < 0.001$; ****: $p < 0.0001$; ns, non-significant. A.U., arbitrary units. (F) HEK293T cells were co-transfected with ORF2-HA or ORF2-2R/2A-HA and TBK1-V5 and lysed 24 h post-transfection. Anti-HA co-IP and WB analysis for TBK1 (anti-V5 staining), ORF2 (anti-HA staining), and β-actin were performed. Shown is a representative blot of n = 3 independent biological experiments.

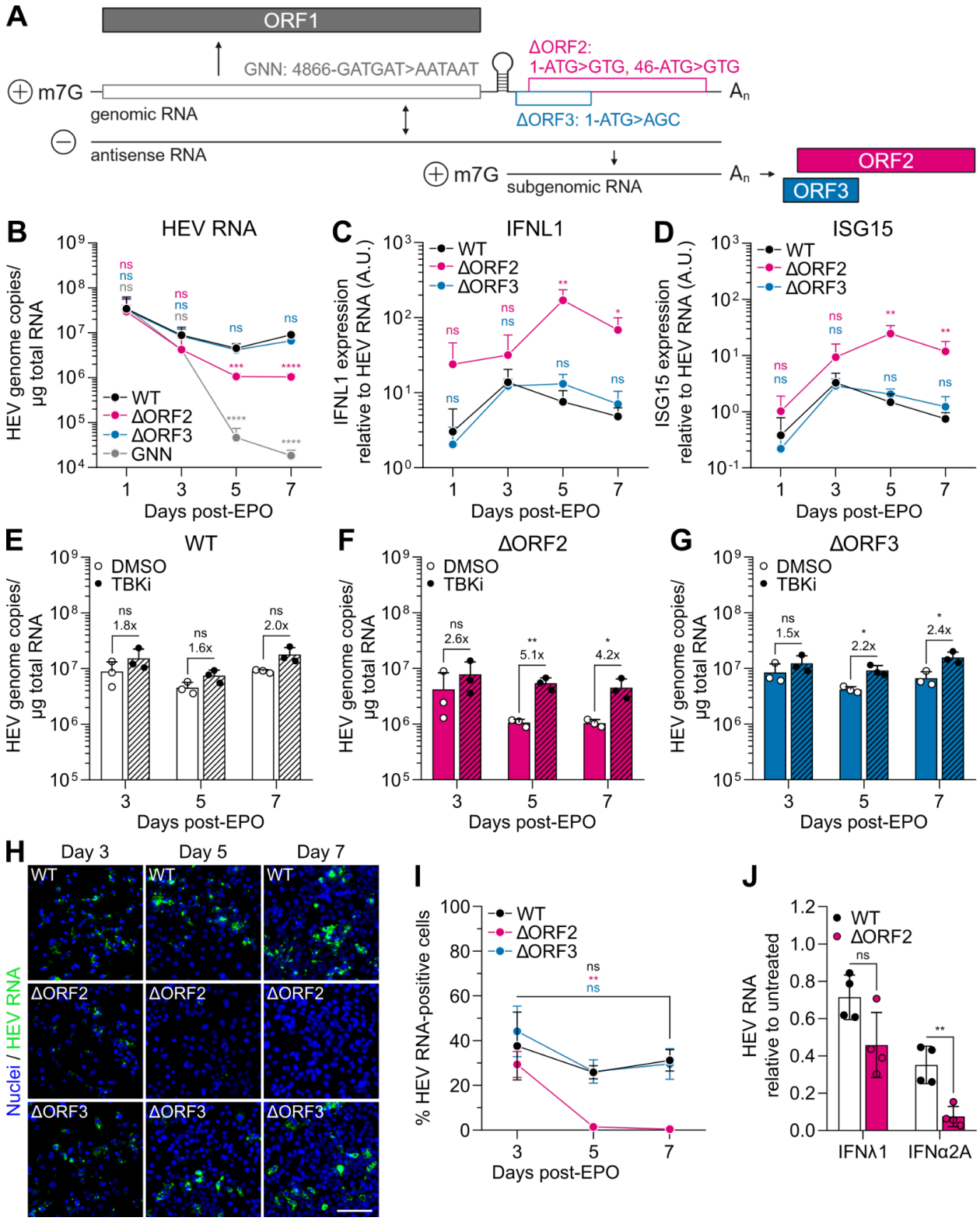

Figure 2: The capsid protein ORF2, but not the ORF3 protein, is pivotal for efficient HEV replication in immunocompetent cells.

(A) Schematic representation of the HEV genome and its replication intermediates. Nucleic acid positions of GNN mutation and start codon mutations of ΔORF2 and ΔORF3 mutants are indicated. m7G, 7-

methylguanosin cap; A_n, poly(A)-tail. Created in BioRender. Dao Thi, V. (2025) https://BioRender.com/j85i934 (B) HepG2/C3A cells were electroporated with *in vitro* transcribed (IVT) HEV WT, ΔORF2, ΔORF3, or replication-incompetent GNN RNA and analyzed by RT-qPCR at indicated time points post-EPO for HEV RNA, (C) *IFNL1* expression normalized over HEV RNA, and (D) *ISG15* expression normalized over HEV RNA. Data show mean ± SD of n = 3 independent biological experiments. Statistical analysis was performed using one-way ANOVA of each time point independently. *: $p < 0.05$; **: $p < 0.01$; ***: $p < 0.001$; ****: $p < 0.0001$; ns, non-significant. A.U., arbitrary units. (E-G) Electroporated HepG2/C3A cells from (B) were additionally treated with 6 μM of the TBK1 inhibitor BX795 (TBKi) or respective DMSO vehicle control 48 h prior to the indicated time point post-EPO. HEV RNA was quantified by RT-qPCR and fold changes over DMSO treatment are shown above the respective graphs. Data show mean ± SD of n = 3 independent biological experiments. Statistical analysis was performed using unpaired two-tailed Student's t-test of each time point independently. *: $p < 0.05$; **: $p < 0.01$; ns, non-significant. (H) Electroporated HepG2/C3A cells from (B) were stained for HEV RNA using RNA-FISH at indicated days post-EPO. Images show exemplary images of n = 3 independent biological experiments. Scale bar, 100 μm. (I) The percentages of electroporated HepG2/C3A cells positive for HEV RNA, stained by RNA-FISH in (H), were quantified with ilastik and CellProfiler. Data show mean ± SEM of 3 independent biological experiments and 5 images quantified per experiment. Statistical analysis was performed using unpaired two-tailed Student's t-test of each condition independently. **: $p < 0.01$; ns, non-significant. (J) Huh7.5 cells were electroporated with IVT HEV WT or ΔORF2 RNA and treated with 10 ng/mL IFNλ1 or 10,000 IU/mL IFNα2A from day 4 to day 7 post-EPO. IFNs were replenished every 24 h. HEV RNA was quantified by RT-qPCR at day 7 post-EPO and normalized over the respective untreated condition. Data show mean ± SD of 4 biological repeats from 2 independent biological experiments. Statistical analysis was performed using unpaired two-tailed Student's t-test of IFNλ1 and IFNα2A independently. **: $p < 0.01$; ns, non-significant.

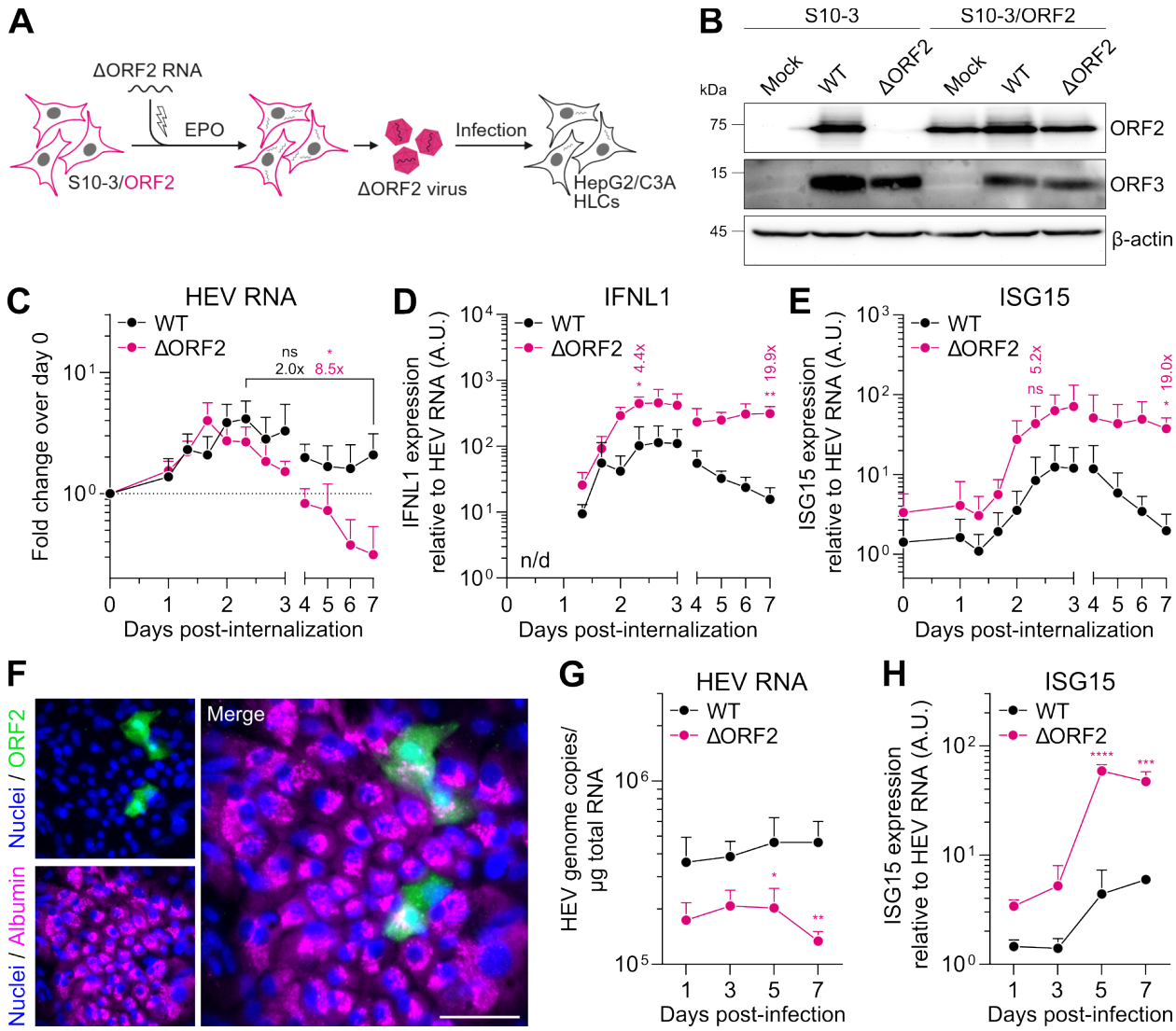

Figure 3: A balance between HEV replication and the antiviral response at an early infection bottleneck is essential for sustained viral replication.

(A) Schematic of ΔORF2 trans-complementation. S10-3 cells stably expressing HEV ORF2 were electroporated with ΔORF2 HEV RNA to produce virus particles containing the ΔORF2 genome packaged in capsid ORF2 protein expressed by the producer cell. Trans-complemented ΔORF2 virus was then used to infect HepG2/C3A cells or stem cell-derived HLCs. Created in BioRender. Dao Thi, V. (2025) https://BioRender.com/u54x394 (B) WB analysis of Mock, WT-, or ΔORF2-electroporated S10-3 or S10-3/ORF2 cells for ORF2, ORF3, and β-actin protein expression. (C) Equal genome copies of HEV WT and ΔORF2 virus particles (30 GE/cell) were bound on HepG2/C3A cells for 2 h at 4 °C prior to internalization at 37 °C for 8 h, followed by removal of inoculum (= day 0). RT-qPCR was performed at indicated time points post-internalization to determine fold viral replication over day 0, (D) *IFNL1* expression normalized to HEV RNA, and (E) *ISG15* expression normalized to HEV RNA. Statistical analysis of fold changes over time (C) or ΔORF2 over WT (D-E) are indicated above the respective time points in the corresponding color. A.U., arbitrary units. Data show mean ± SD of n = 3 independent biological experiments. Statistical analysis was performed using unpaired two-tailed Student's t-test of the respective conditions or days independently. *: $p < 0.05$; **: $p < 0.01$; ns, non-significant. n/d, non-detectable; A.U., arbitrary units. (F) Exemplary image of stem cell-derived hepatocyte-like cells (HLCs) infected with HEV WT, fixed, and stained for albumin and ORF2 by immunofluorescence. Scale bar, 50 µm. (G) Stem cell-derived HLCs were infected with equal genome copies of HEV WT and ΔORF2 virus particles (30 GE/cell) and analyzed by RT-qPCR for HEV

918 RNA and (H) *ISG15* expression normalized to HEV RNA over time. Data show mean ± SD of n = 4 biological
919 replicates of two independent HLC differentiations. Statistical analysis was performed using unpaired two-
920 tailed Student's t-test of each time point independently. *: $p < 0.05$; **: $p < 0.01$; ***: $p < 0.001$; ****: $p <$
921 0.0001; ns, non-significant.

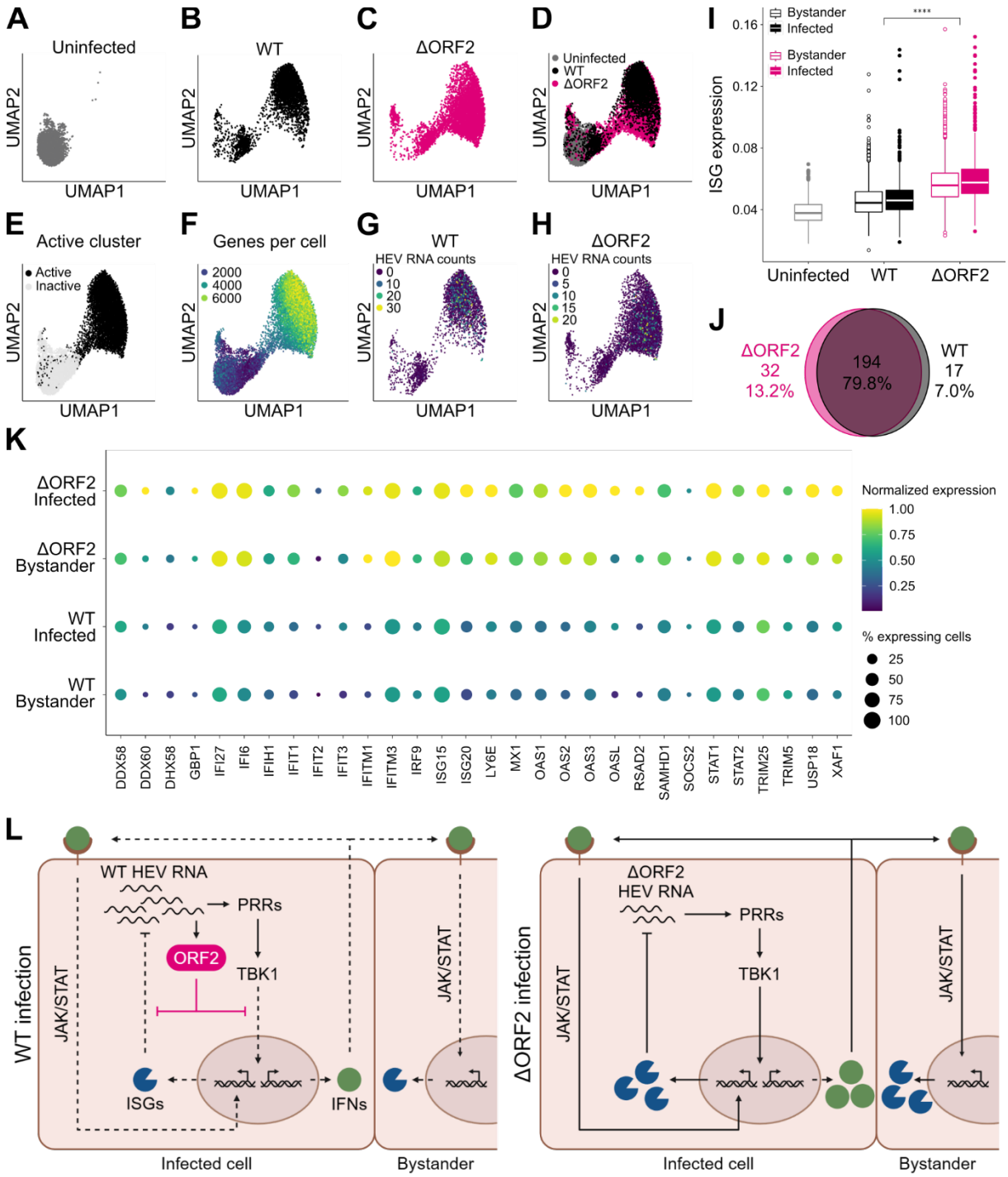

Figure 4: scRNA-seq analysis reveals ISG responses in HEV-infected cells and bystanders which are dampened in the presence of ORF2.

(A) UMAP projections of uninfected, (B) WT-infected, or (C) ΔORF2-infected HepG2/C3A cells harvested at 56 h post-synchronized infection and processed by microfluidics-based 3'-targeted 10x Genomics. UMAPs were generated by clustering of all cells based on a list of approximately 400 ISGs published previously by Schoggins *et al.*[40] (D) Combined UMAP projections of uninfected, WT-, and ΔORF2-infected

samples, colored by condition. (E) Cells with upregulated ISG expression were highlighted in UMAP projections of uninfected, WT-, and ΔORF2-infected samples in black, representing the active cluster. (F) UMAP projection of uninfected, WT-, and ΔORF2-infected samples, highlighting the number of genes detected per cell in all samples. (G) UMAP projections of the WT-infected and (H) ΔORF2-infected samples with indicated HEV RNA counts. (I) Global changes in the ISG response were analyzed by comparison of normalized ISG expression across all samples (Uninfected, WT, and ΔORF2), based on a list of approximately 400 ISGs. WT- and ΔORF2-infected samples were split into actively infected cells, defined by detection of at least one HEV RNA copy per cell, and uninfected bystanders. Statistical analysis was performed using a two-sided Wilcoxon rank sum test. ****: $p < 0.0001$. (J) Differentially expressed ISGs in the active clusters of WT- and ΔORF2-infected samples were compared and plotted in a Venn diagram. Absolute numbers and percentages of shared and distinct differentially expressed ISGs are shown. (K) Out of the overlapping, differentially expressed ISGs between the active clusters of WT- and ΔORF2-infected samples, 30 ISGs were selected. Normalized expression and the percentage of cells were plotted for only the active clusters (as shown in E) of WT- and ΔORF2-infected samples, split by actively infected cells (at least one HEV RNA count per cell) and uninfected bystanders. (L) Working model depicting direct interference of ORF2 with TBK1 signaling downstream of PRR recognition of HEV RNA in WT-infected cells. Consequently, ISG induction downstream of PRR signaling as well as IFN secretion and thus, autocrine and paracrine ISG induction downstream of the IFN receptor is dampened in infected cells and bystanders, respectively. Additionally, ORF2 shields HEV RNA from the antiviral functions of ISGs. In ΔORF2-infected cells, the lack of the antagonistic functions of ORF2 results in stronger ISG induction downstream of PRR signaling as well as enhanced IFN secretion, resulting in stronger autocrine and paracrine ISG induction downstream of IFN signaling. Viral replication is consequently dampened as a result of the actions of antiviral effectors. Created in BioRender. Dao Thi, V. (2025) https://BioRender.com/h01q004